Statics and Dynamics of Adhesion between Two Soap Bubbles

Sébastien Besson, Georges Debrégeas

EPJ manuscript No.
(will be inserted by the editor)

Statics and dynamics of adhesion between two soap bubbles

S. Besson, G. Debrégeas

Laboratoire de Physique Statistique, CNRS UMR 8550,
24, rue Lhomond, 75231 Paris Cedex 05, France

August 10, 2007

Abstract An original set-up is used to study the adhesive properties of two hemispherical soap bubbles put into contact. The contact angle at the line connecting the three films is extracted by image analysis of the bubbles profiles. After the initial contact, the angle rapidly reaches a static value slightly larger than the standard $120°$ angle expected from Plateau rule. This deviation is consistent with previous experimental and theoretical studies: it can be quantitatively predicted by taking into account the finite size of the Plateau border (the liquid volume trapped at the vertex) in the free energy minimization. The visco-elastic adhesion properties of the bubbles are further explored by measuring the deviation $\Delta\theta_d(t)$ of the contact angle from the static value as the distance between the two bubbles supports is sinusoidally modulated. It is found to linearly increase with $\Delta r_c/r_c$ where r_c is the radius of the central film and Δr_c the amplitude of modulation of this length induced by the displacement of the supports. The in-phase and out-of-phase components of $\Delta\theta_d(t)$ with the imposed modulation frequency are systematically probed, which reveals a transition from a viscous to an elastic response of the system with a crossover pulsation of the order 1rad.s^{-1}. Independent interfacial rheological measurements, obtained from an oscillating bubble experiment, allow us to develop a model of dynamic adhesion which is confronted to our experimental results. The relevance of such adhesive dynamic properties to the rheology of foams is briefly discussed using a perturbative approach to the Princen 2D model of foams.

PACS. 47.55.D- Drops and bubbles – 47.55.dk Surfactant effects – 83.80.Iz Emulsions and foams

1 Introduction

Liquid foams are concentrated dispersions of gas bubbles in a liquid matrix. Their mechanical properties have been the focus of a number of studies in the recent past [1,2,3]. Liquid foams exhibit quasi-elastic behavior up to a finite yield stress or strain beyond which they flow like shear-thinning viscous fluids. Most of the elastic response originates from the variation of the total film area induced by an applied shear. The resulting shear modulus scales as $\mu = 2\gamma/R$ where 2γ is the surface tension of the soap film, and R the average radius of the bubbles. The dissipation is controlled, in major part, by irreversible rearrangements of the bubbles (T1 events).

Other mechanisms of energy storage and dissipation however contribute to the viscoelastic moduli of the foam. They have been thoroughly discussed theoretically [4,5]. One is associated with the interfacial viscoelasticity of the soap films, which can be independently measured using a wide range of experimental techniques (oscillating barriers [6,7], thin-film interfaces [8], oscillating bubble/drop [9,10,11]). They all consist in submitting a single mono- or bi-layer to an oscillating stretching while measuring the evolution of the surface tension. The second source of dissipation takes place in the Plateau borders, the region of the foam where the films meet and where most of the liquid content is trapped. As the foam is strained, the Plateau borders move relatively to the soap films to which they are connected, inducing dissipative viscous flows. This viscous drag force has been extensively studied but only in a situation where the Plateau border is in contact with a solid surface [12,13,14,15].

Relating these local measurements (interfacial rheology and Plateau border viscous drag force) to the global rheology of the foams is tricky. First, it is difficult to actually separate the different modes of dissipation. In a real foam, Ostwald ripening (the disproportionation of bubbles induced by gas diffusion through the films) induce T1 events even in the absence of an imposed strain. Second, due to the many modes of accessible deformation, the motion of the vertices in a foam under simple strain is not affine. Describing their trajectory becomes extremely difficult when the foam is polydisperse.

Beyond these issues, one can also question the relevance of measurements performed with an isolated film to describe the behavior of a macroscopic foam. In all the techniques currently used to estimate the rheological properties of the films, the surfactant layers are confined by solid barriers. In contrast, films in a real foam are bounded by fluid Plateau borders which may allow the transfer of surfactants from one side to another. In the case of Plateau borders viscous drag, the situation is even worst: the resistance to motion is measured by dragging a Plateau border along a solid wall, which imposes a very different hydrodynamic boundary to the flow by comparison with a self supported Plateau border.

One attempt to extract information about local dissipation within a macroscopic foam has been recently proposed by Du-

rand and Stone [16]. They optically studied the dynamic of T1 events in a confined 2D foam (a monolayer of bubbles squeezed between two solid plates) and were able to relate the duration of the plastic process with intrinsic rheological properties of the soap films. This experiment enables the authors to study plastic processes *in situ*, although it is limited to a confined geometry. But the use of T1 events as the deformation mechanism does not allow one to modulate in a controlled way the dynamics of local deformation of the set of bubbles (although this might actually be feasible with minor modification of the authors' experimental procedure).

In this article, we propose a new approach to study local elastic and dissipative processes in a configuration more directly amenable to 3D foams. Two hemispherical bubbles are put into contact and their relative distance is modulated at various frequencies. In this configuration, the central film separating the two bubbles is bounded by a self-supported Plateau border whose radius oscillates with the distance between the two bubbles supports. We focus on angular measurements at the contact line which provide most of the relevant information concerning the elastic and dissipation processes.

The article is organized as follows. In part 2, the experimental set-up, the optical measurements and image analysis procedure are detailed. The static results of contact angle measurements are presented in part 3, together with data obtained from a numerical simulation. Part 4 focuses on dynamic properties of adhesion and also presents the results of standard rheological interfacial measurements performed on single films using the same soap solution. These results are discussed in part 5: a microscopic model, which describes the transport of surfactant molecules between the interfaces and the bulk as well as between adjacent interfaces, is developed. Its prediction in terms of angular moduli is confronted to the experimental measurements. In part 6, the consequence of this angular response for the rheology of foams is discussed within the scope of the Princen 2D hexagonal model [17]. Conclusion and perspectives are drawn in part 7.

2 Experiments

An hemispherical bubble is formed by blowing air at the cone-shaped end of a stainless steel tube, of external radius $R = 7$mm, filled with a soap solution (figure 1). The liquid in the tube is connected through a porous disk (Duran, diameter 2.8mm, height 5mm) to a reservoir. Once the bubble is formed, the reservoir is lowered a few centimeters to impose a small negative pressure difference between the liquid and gas phases. The disk porosity is fine enough (poresize 10-16μm) to prevent the bubble from being sucked down. The entire device is enclosed in a glass cell ($40\times40\times40$cm) to limit evaporation and increase the bubbles lifetime. In all the experiments, the soap solution is made of tetramethyltetradecylammonium bromide (TTAB purchased from Sigma-Aldrich) 3g/L in a water/glycerol mixture (volume ratio of 75/25).

This device is used in two types of experiments. In single bubble experiments, a section of the air tube is squeezed between two plates whose separation can be sinusoidally modulated using a DC motor (Newport, LTA-HS). A pressure sensor (Validyne, DP103) allows us to simultaneously monitor the pressure drop between the inside and outside of the bubble. In the double bubble setup, a similar device is placed on top of the first one (figure 1) and their axis are carefully aligned. The top device is mounted on a vertical displacement stage attached to the DC motor.

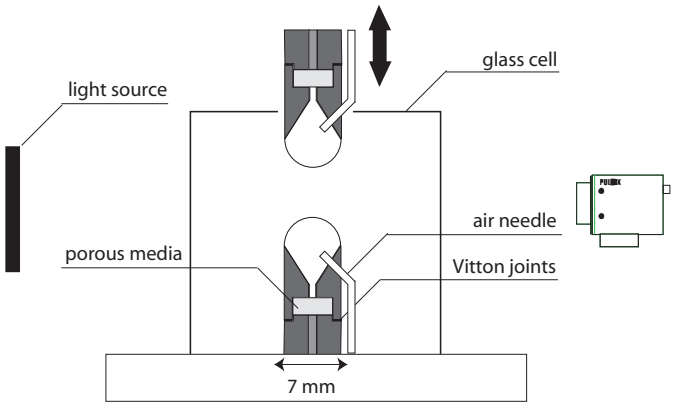

Figure 1. Schematic of the experimental double bubble device.

The set-up is illuminated by a diffusive light source (Schott, Backlight). The shadow image of the bubbles is captured on a CCD-camera equipped with a telecentric objective (Navitar, 6X) to allow accurate angular and length measurements. Depending on the studied frequency, two cameras are used: a Pulnix TM-1320 CL and a Mikrotron MC1310 with frame rates up to 15 frames/s and 240 frames/s respectively. Image capture is synchronized with the motor motion and pressure recording. The bubbles profiles are extracted by image analysis with a subpixel resolution using the software IDL (see figure 2(c)). The symmetry axis is determined and defines the cylindrical coordinates (r, z). For both bubbles, the profiles $r(z)$ are fitted to the Young-Laplace equation which relates the local curvature $\frac{1}{R'} + \frac{1}{R''}$ to the pressure drop ΔP across the film:

$$\Delta P = 2\gamma(\frac{1}{R'} + \frac{1}{R''}) \tag{1}$$

The profile equation $r(z)$ thus obeys the differential equation:

$$\frac{r(z)}{\sqrt{1 + r'(z)^2}} = \frac{\Delta P}{4\gamma} r(z)^2 + \lambda \tag{2}$$

where 2γ is the surface tension of the soap film; the parameter λ results from the integration of equation (1) and is set by the boundary conditions. For each bubble, the set of parameters $\left(\frac{\Delta P}{4\gamma}, \lambda\right)$ is extracted from the best fit of the region of the profiles outside the Plateau border. The prolongations of the reconstructed profiles intersect in the Plateau border and define a contact radius r_c and a contact angle θ as shown in figure 2(c). Similarly, the three interfaces which delimit the Plateau border obey the same equation (2) with the term $\frac{\Delta P}{4\gamma}$ replaced by $\frac{\Delta P}{2\gamma}$ since these are single air/water interfaces. Here ΔP corresponds to the pressure difference between the liquid in the Plateau border and the gas phase (bubble or atmosphere).

By fitting the external profile, we extract the set of parameters $\left(\frac{\Delta P}{2\gamma}, \lambda_l\right)$ and reconstruct the Plateau border (see figure 2(d)).

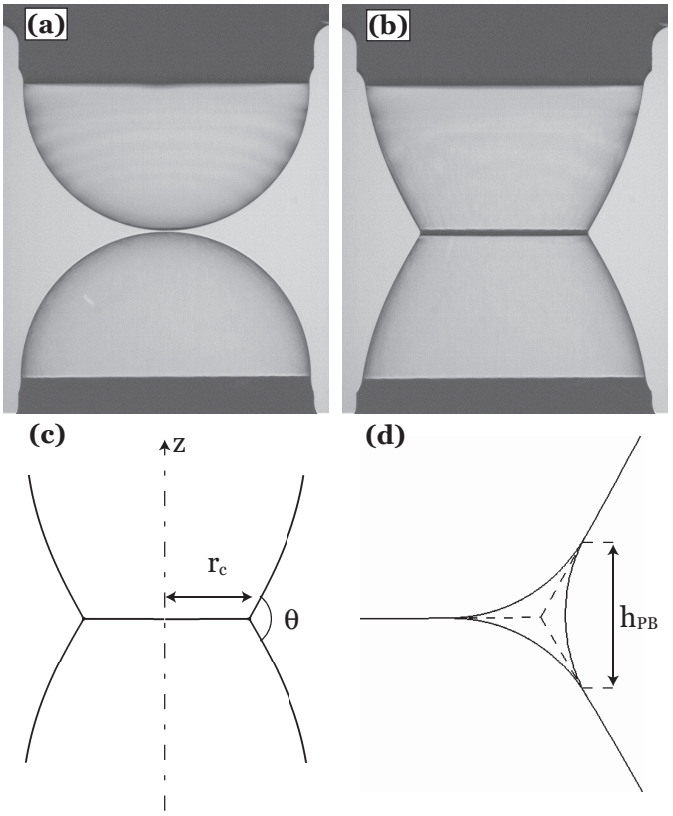

Figure 2. Images of a double bubble static adhesion experiment (a) before contact and (b) just after contact. Results of the image analysis: (c) external profiles fitted by the Young-Laplace equation from which the central film radius r_c and contact angle θ are extracted, (d) reconstructed Plateau border. The height h_{PB} is defined as the distance between the top and bottom intersection points of the Plateau border interfaces.

3 Dynamics of first contact and static equilibrium angle

Two bubbles are brought into contact at vanishing low speed. Time 0 is defined by the recording time of image of the first contact. The time evolution of the central film radius r_c and contact angle θ at short times are shown on figure 3. It exhibits a transient of a few seconds during which both parameters significantly vary. The first ~ 0.1s corresponds to the rapid formation of the central film: only the end of this phase can be captured even with the fast camera. During the next few seconds, the radius and contact angle keep increasing. This second stage is associated with the capillary drainage of the freshly formed film toward the Plateau border which allows pressure equilibration within the liquid phase. This process can be monitored by measuring the evolution of the Plateau border height h_{PB} (see figure 2(d) for its definition) which appears to evolve with the same characteristic time as the contact radius (figure 3). For $t \gtrsim 10$s, the system is equilibrated but a slow decay of r_c is still observable due to gas diffusion through the films (figure 4). This process does not affect the value of the contact angle θ which remains constant until the bubbles break up (after a few minutes).

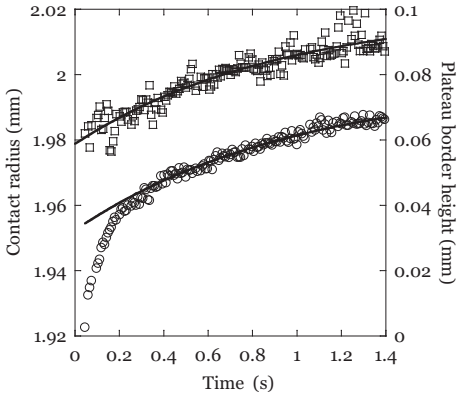

Figure 3. Short-times evolution of the contact radius (circles) and the Plateau border height (squares) as a function of time for two contacting bubbles. During the first 0.2s, the fast rise of the contact radius conrresponds to the initial growth of the central film. After 0.2s, the evolution of the contact radius is to be compared to the one of the Plateau border height. Both series of measurements are adjusted by rising exponential fits of the type $x_0 + \Delta x(1 - e^{\frac{-t}{\tau}})$ (solid lines) and highlight a characteristic time τ of the order of 1s.

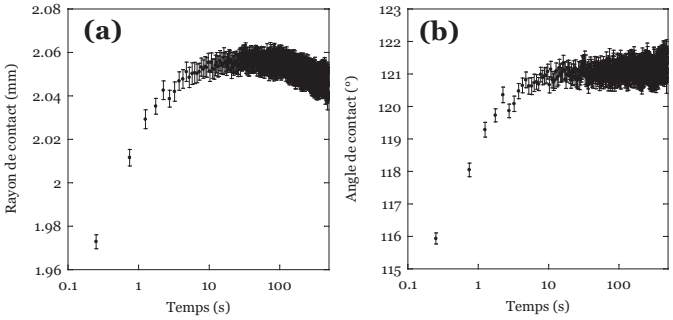

Figure 4. Long-times evolution of (a) the contact angle and (b) the contact radius as a function of the time during a contacting bubbles experiment. After an initial growth, both series reach constant values, the contact angle value being slightly higher than the predicted 120° from the Plateau rule. The decay of the contact radius after 60s is attributed to the gas diffusion outside the bubble. The experiment ends up when one of the two bubbles break.

We define θ_∞ as the value of the contact angle for time $t >$10s. For all experiments, θ_∞ is found to be larger than $120°$, the value predicted by Plateau rule [18]. Such a deviation has been previously observed in various experiments [19, 20, 21]. In the last reference, similar measurements were performed on a single catenoid separated by a soap film. The contact angle between both catenoidal films was found to grow linearly with

the ratio $\frac{r_{PB}}{r_c}$ where r_{PB} is the Plateau border curvature radius and r_c the central film radius.

This deviation can be qualitatively understood by first considering an infinitely dry foam. In this case, the force equilibrium at the contact line imposes the three films to meet at 120°. Decorating the line with a Plateau border reduces the total area of the films by a quantity $2S_{dry} - S_{PB}$ [22] which is a (negative) decreasing function of the Plateau border volume. The presence of a Plateau border is thus associated with a negative line tension. In the specific case of the double bubble, this effect has been described by Fortes and Teixeira [23]. They predict a contact angle in the presence of Plateau border given by:

$$\theta_{stat} = 120 + \frac{180}{\pi}\frac{1}{4\pi r_c^2\sqrt{3}}(2S_{dry} - S_{PB}) \qquad (3)$$

In order to test this expression, several contacting bubbles experiments are performed with different values of contact radius and Plateau border height. When the top bubble is initially formed, a liquid droplet is suspended at its apex. After contact, part of this liquid gathers in the Plateau border but a fraction of it flows down the lower bubble. If one separates the two bubbles then brings then into contact again, part of the liquid is further eliminated. The Plateau border size can thus be varied by applying successive contacts and separations of the bubbles. For each experiment, the final value of the contact angle as well as $S_{dry} - S_{PB}$ are measured. Figure 5 shows the measured angle θ_{stat} as a function of the prediction of equation (3).

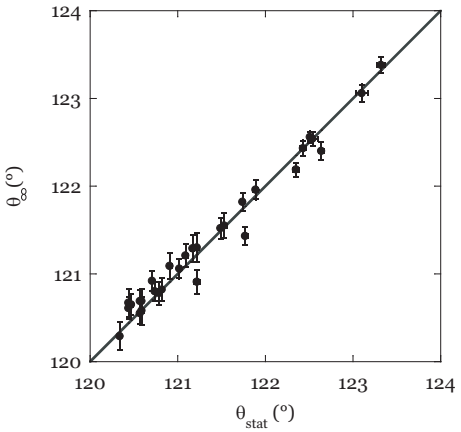

Figure 5. Experimental static contact angle θ_∞ as a function of the angle predicted by Fortes law θ_{stat} (equation 3) for various values of the radius r_c and the Plateau border volume. Each data point corresponds to the average of angular measurements performed after 10s of contact.

It should be noticed that this model ignores disjoining pressure effects such as those reported in references [24,25]. Although gravity drainage tends to decrease the films thickness, this process is largely slowered in our experiment by the presence of glycerol in the solution. The thickness of the films have not been measured, but in all experiments, the films diffuse light which indicates that their thickess is larger than ~ 1 μm. In this range, disjoining pressure are negligeable. Consistently, we do not observed any evolution of the contact angle with time beyond ~ 10 s after initial contact.

This result was independently confirmed by simulations of the double bubble experiment carried out using Surface Evolver [26]. This software allows one to calculate minimal surface configurations under a given set of conditions. Two contacting bubbles of fixed volume are generated with different volumes of the Plateau border. After several minimization cycles, the equilibrated configuration is treated the same way as for the experiments. Figure 6 shows the numerical contact angle versus the predicted contact angle value for various Plateau border volumes.

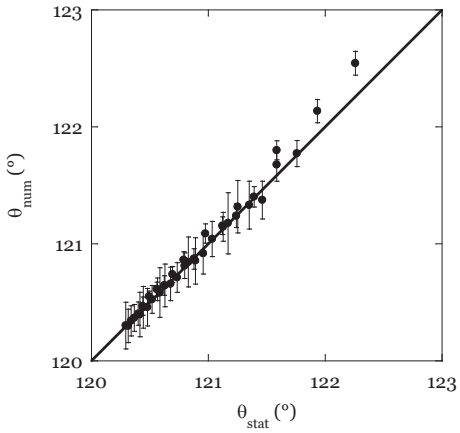

Figure 6. Numerical contact angle θ_{num} obtained from Surface Evolver simulations as a function of the angle predicted by Fortes law θ_{stat} (equation 3) for various values of the imposed Plateau border volume.

The agreement of the experimental and numerical results with Fortes and Teixeira's model validates the decoration law for the double bubble. It also demonstrates the accuracy of the angle measurement procedure. In the rest of the article, expression 3 will be used in order to calculate, at any moment, the equilibrium contact angle $\theta_{stat}(t)$. This reference angle will be subtracted from the measured angle in order to extract the dynamic deviation $\Delta\theta_d = \theta(t) - \theta_{stat}(t)$.

4 Dynamics of adhesion

In order to probe the dynamic response of the contact angle, a sinusoidal displacement of the upper tube is applied at controlled pulsations in the range 0.01-20 rad.s^{-1}. The double bubble system is prepared as previously described. All experiments are performed with a contact radius $r_c \approx 2$mm and a Plateau border height $h_{PB} \approx 0.2\text{mm} << r_c$. Figure 7 shows the typical time evolution of $r_c(t)$ and $\theta(t)$. The corrected contact angle, $\theta_{stat}(t)$ calculated from equation 3, varies between 120.50° and 120.56°. Therefore, the main contribution to the observed oscillation of $\theta(t)$ is due to dynamic effects. The evolution of these two parameters are decomposed as:

$$r_c(t) = r_{c0} + \Delta r_c(\omega) cos(\omega t) \quad (4)$$

$$\Delta\theta_d(t) = \Delta\theta(\omega) cos(\omega t + \phi(\omega)) \quad (5)$$

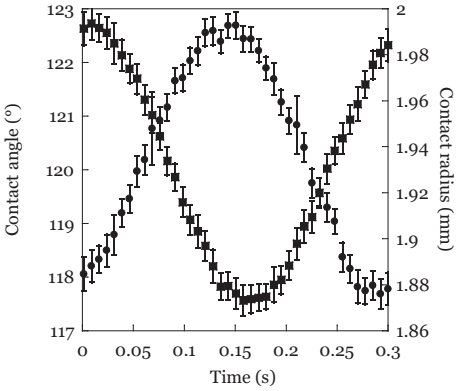

Figure 7. Evolution of the contact radius (squares) and the contact angle (circles) as a function of the time over an oscillating period for an oscillating amplitude of 0.2mm at a pulsation of 20rad.s^{-1}. The error bars are calculated from the uncertainties on the fitting parameters (equation 2). Typical standard deviations are equal to 7μm for the contact radius and $0.2°$ for the contact angle.

It should be noted that r_{c0} is not strictly constant : it slightly decreases as a consequence of the gas diffusion (figure 4(b)). To precisely measure $r_c(\omega)$, $\Delta\theta(\omega)$ and $\phi(\omega)$, $r_c(t)$ and $\Delta\theta_d(t)$ are therefore filtered to extract the Fourier component associated with the imposed frequency. Figure 8 shows the dependence of $\Delta\theta$ with $\Delta r_c/r_{c0}$ for three different oscillation frequencies. It shows that the contact angle response is linear with the imposed solicitation. This allows one to define two moduli associated with the in-phase and out-of-phase responses of the contact angle to the modulation of the contact radius:

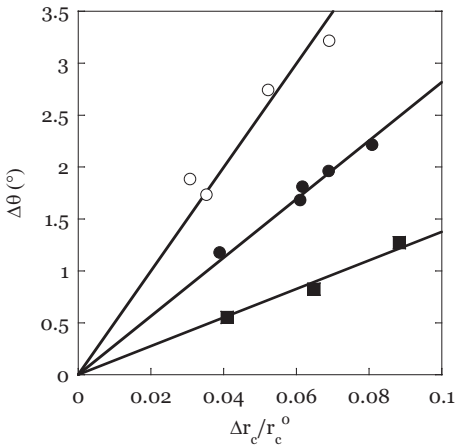

Figure 8. Linearity of the amplitude of the dynamic angle deviation with the amplitude of the normalized contact radius variations at different frequencies. Squares: 0.2rad.s^{-1}. Circles: 1rad.s^{-1}. Diamonds: 5rad.s^{-1}.

$$A'(\omega) = -\frac{\Delta\theta(\omega)}{\Delta r_c(\omega)} r_{c0} cos(\phi(\omega)) \quad (6)$$

$$A''(\omega) = -\frac{\Delta\theta(\omega)}{\Delta r_c(\omega)} r_{c0} sin(\phi(\omega)) \quad (7)$$

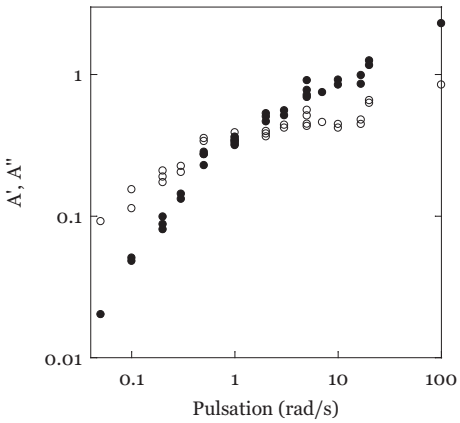

Figure 9. Evolution of the angular elastic and viscous moduli, estimated from equation (6) and (7), with the frequency of the oscillation. Closed circles: elastic modulus. Open circles: loss modulus.

Figure 9 shows the evolution of A' and A'' as the pulsation ω is varied over 3 decades. It reveals a transition from a viscous regime at low frequency to an elastic regime at high frequency, with a crossover around 1rad.s^{-1}..

The existence of an in-phase component of the dynamic angle signal cannot be accounted for by dissipation in the Plateau border alone. In contrast, it can be understood by considering the viscoelastic behavior of the soap films [27,16]. As the distance between the bubbles are modulated, the films area varies which in turn induces a variation of their surface tension. In Gibbs approach, the surface tension $\gamma(t)$ associated with a sinusoidal modulation of the film surface area $S(t) = S^0 + \Delta S cos(\omega t)$ is written, in the limit $\Delta S/S^0 \approx 0$:

$$\gamma(t) = \gamma_0 + E'(\omega)\frac{\Delta S}{S_0} cos(\omega t) + E''(\omega)\frac{\Delta S}{S_0} sin(\omega t) \quad (8)$$

where $E^*(\omega) = E'(\omega) + iE''(\omega)$ is the dilational complex modulus [28]. This parameter can be independently evaluated by sinusoidally modulating the volume of a single bubble while recording its radius R and the difference between the inside and the outside pressure ΔP, from which its surface tension is determined using the Young-Laplace relation $2\gamma = \Delta P/2R$. The frequency diagram of both moduli are plotted on figure 10.

Both elastic and viscous moduli exhibit a similar increase with the pulsation in $\sqrt{\omega}$ (as shown by the solid line in figure 10). Such a behavior of the dilational moduli has been predicted by Lucassen, in the limit of low frequency, for solutions below [6] and above [29] the critical micellar concentration. In these models, the surfactants adsorption at the interface is limited by diffusion in the bulk. This process defines a characteristic time set by the physico-chemical properties of the bulk solution.

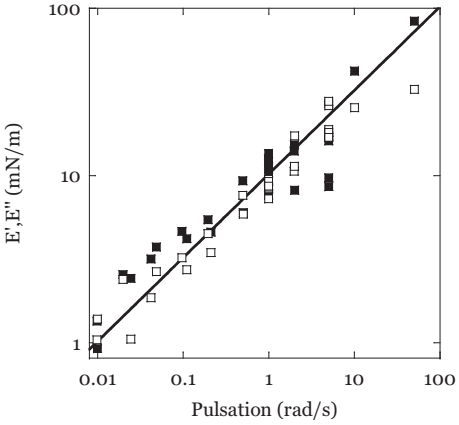

Figure 10. Evolution of the dilational elastic and viscous moduli with the frequency of the oscillation for an oscillating bubble experiment. Closed squares: elastic modulus. Open squares: viscous modulus. The dispersion is mainly due to uncertainties on the measurement of the internal pressure. Experimental data are fitted by the expressions of the Lucassen model above the critical micellar concentration (solid line).

5 Interpretation

In this section, we attempt to relate the double-bubble angular measurements to the film rheological moduli obtained from the single oscillating bubble experiment. In order to do so, we separately describe the evolution of each monolayer characterized at each time by their area and surface tension denoted S_i and γ_i respectively (see figure 11)[1].

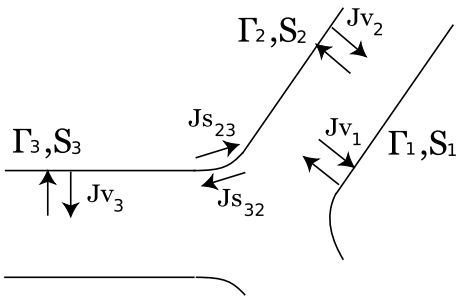

Figure 11. In the case of a double bulle, one needs to consider 3 surfaces characterized by (S_i, γ_i) . Each monolayer exchanges with the bulk solution with a flux Jv_i and with adjacent surface with a Marangoni flux Js_{ij}.

As the distance between the bubbles supporting cones is modulated, each monolayer experiences cycles of compression and stretching which in turn modulate its surface tension γ_i. We define the instantaneous deviation $\Delta\gamma_i$ to the equilibrium surface tension γ_0 such as $\gamma_i = \gamma_0 + \Delta\gamma_i$. In the limit of $\Delta\gamma_i \ll \gamma_0$, mechanical equilibrium at the intersecting line between the three interfaces imposes:

$$\Delta\theta = \frac{1}{\gamma_0\sqrt{3}}(\Delta\gamma_1 + \Delta\gamma_2 - 2\Delta\gamma_3) \tag{9}$$

We now write the conservation of mass of surfactants for each monolayer in the form of:

$$S\frac{d\Gamma}{dt} + \Gamma\frac{dS}{dt} = J_v + J_s \tag{10}$$

where Γ is the surface concentration of the surfactant. The first flux J_v characterizes the exchange between the liquid phase and the interface while J_s corresponds to the exchange of surfactants between adjacent monolayers (Marangoni flow).

For a single oscillating bubble, J_v is the only relevent flux. The quantities γ_i and S_i are coupled through equation 8, and from equation 10, the volumic flow Jv can be expressed as a function of the dilational elastic module E^* through:

$$Jv = S\frac{d\Gamma}{dt}\left(1 - \frac{E_0}{E^*}\right) \tag{11}$$

where

$$E_0 = -d\gamma/d\ln(\Gamma) \tag{12}$$

In the case of the double bubble, the transfer of surfactants between the monolayers 2 and 3 has to be taken into account through the flux J_s. One should in principle consider the concentration Γ_i as a continuously varying quantity. Here, we make the simplifying assumption that one can still consider that each monolayer can be characterized by a single surface tension and that the surface flux Js can be written as:

$$Js_{23} = -J_{32} = D_S\frac{\Gamma_2 - \Gamma_3}{L}2\pi r_c \tag{13}$$

where D_s is the surface diffusion coefficient of the surfactant and L a characteristic length of the order of the bubbles radius. From these two expressions, the mass conservation equation 10 for the three interfaces now reads:

$$E_0 S_1\frac{d\Gamma_1}{dt} = -\Gamma_1 E^*\frac{dS_1}{dt} \tag{14}$$

$$E_0 S_2\frac{d\Gamma_2}{dt} = -\Gamma_2 E^*\frac{dS_2}{dt} + E^* D_S\frac{\Gamma_3 - \Gamma_2}{L}2\pi r_c \tag{15}$$

$$E_0 S_3\frac{d\Gamma_3}{dt} = -\Gamma_3 E^*\frac{dS_3}{dt} + E^* D_S\frac{\Gamma_2 - \Gamma_3}{L}2\pi r_c \tag{16}$$

Using expression 12, this system of coupled equations 14, 15 and 16 can be solved to obtain an expression of the surface tension variations $\Delta\gamma_i$ as a function of the surface area variations $\Delta S_i/S_i$:

$$\Delta\gamma_1 = E^*\frac{\Delta S_1}{S_{10}} \tag{17}$$

$$\Delta\gamma_2 = E^*\frac{iE_0\omega\tau}{E^* + iE_0\omega\tau}\frac{\Delta S_2}{S_{20}} \tag{18}$$

$$\Delta\gamma_3 = E^*\frac{iE_0\omega\tau}{E^* + iE_0\omega\tau}\frac{\Delta S_3}{S_{30}} \tag{19}$$

[1] the system is assumed to be symmetric with respect to the central film, which is the case in all experiments, so that the upper and lower monolayers have identical characteristics

where τ is a characteristic time of surface tension equilibration between adjacent monolayers defined as:

$$\tau^{-1} = 2\pi \frac{r_{c0}}{L} D_S \frac{S_{20} + S_{30}}{S_{20} S_{30}} \tag{20}$$

Experimental measurements of the different surface areas as well the Surface Evolver simulations show that $S_1(t)+S_2(t)$ is a constant, equal to $2\pi R^2$ for initially hemispherical bubbles. The expression of the areas S_i and their variations ΔS_i are thus simply related, to first order, to the contact radius r_c and its variation Δr_c through the following relationships:

$$S_1 = S_2 = 2\pi R^2 - \pi r_c^2 \tag{21}$$
$$\Delta S_1 = \Delta S_2 = -2\pi \Delta r_c r_{c0} \tag{22}$$
$$S_3 = \pi r_c^2 \tag{23}$$
$$\Delta S_3 = 2\pi \Delta r_c r_{c0} \tag{24}$$

From this, and the expression of $\Delta\theta$ given by equation 9, one can deduce the angular complex modulus $A*$:

$$A^* = \frac{2E^*}{\gamma_0\sqrt{3}} \left(\frac{iE_0\omega\tau}{E^* + iE_0\omega\tau} \frac{4R^2}{2R^2 - r_{c0}^2} + \frac{E^*}{E^* + iE_0\omega\tau} \frac{r_{c0}^2}{2R^2 - r_{c0}^2} \right) \tag{25}$$

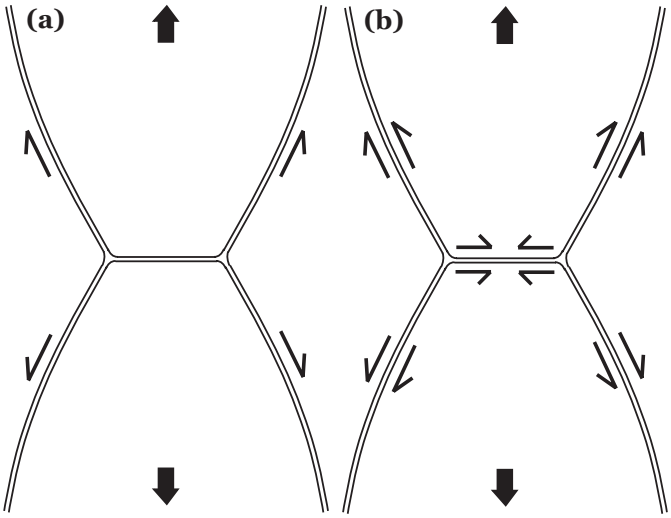

Figure 12. Limiting models of compression/stretching of the monolayers for a double bubble submitted to an oscillating solicitation. (a) When $\omega\tau \ll 1$, surface diffusion processes are fast. Since the internal surface is constant, its surface tension of the internal film does not vary and the only contribution to the contact angle comes from the external monolayer. (b) When $\omega\tau \gg 1$, surface diffusion processes are slow. The surface tension is the same on either side of each film wich responds independently from each other.

Two limiting situations can be identified :

- When $\omega\tau \ll 1$, interfacial diffusion processes are instantaneous so that surface tension are immediately equilibrated between interfaces 2 and 3. In this limit, the interfaces can freely slide one over the other. Since $S_2 + S_3$ is constant, the contact angle deviations are only due to the external surface compression cycles as shown in figure 12 (a). The expression of the complex angular modulus reduces to:

$$A_1^* = \frac{2E^*}{\gamma_0\sqrt{3}} \frac{r_{c0}^2}{2\pi R^2 - \pi r_{c0}^2} \tag{26}$$

- When $\tau \gg 1$, marangoni flows are negligeable and the three double interfaces oscillates independently as shown in figure 12 (b). In this case the expression of the complex angular modulus reads:

$$A_2^* = \frac{2E^*}{\gamma_0\sqrt{3}} \frac{4R^2}{2\pi R^2 - \pi r_{c0}^2} \tag{27}$$

Figure 13 shows the frequency diagram of A' and A" and the two limiting predictions of A^* given by equations 26 and 27 using the Lucassen adjustement of E^*. Consistently, the experimental moduli lay within the limiting models over the whole range of frequency. The best fit of the data using equation 25 is also plotted which corresponds to a characteristic transition time $\tau = 3.10^{-4}s$. Although it compares correctly with the data at low frequency, significant deviation is observed at high frequency.

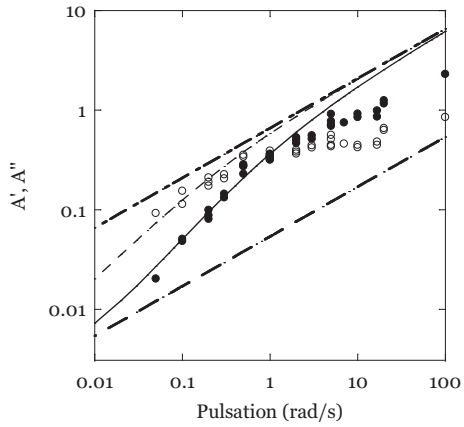

Figure 13. Comparison of the experimental angular moduli A' (closed circles) and A'' (open circle) with the results of the double bubble model adjusted with $\tau = 3.10^{-4}s$. The dashed lines represent the results corresponding to the sliding monolayers model, A_1' and A_2'' (dashed lines), and the independant films model, A_2' and A_2'' (dashed dot lines).

6 Application to a 2D model foam

In this part, the consequence of such dynamic effects on the bulk rheology of foams is discussed. We attempt to estimate how the angular measurements provided by the double bubble set-up can be relevant to predict the contribution of the films (and Plateau borders) to the foam rheological properties. Such effects has been evidenced in macroscopic foam measurements

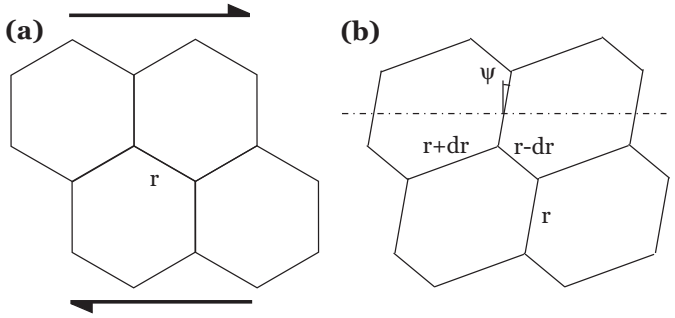

Figure 14. The Princen model for the deformation of a 2D hexagonal foam. (a) Initial configuration. (b) After a small quasistatic deformation, the angles of the Plateau border remain equal to 120°. To the first order, the vertical films length remains unchanged but their orientation change by an angle ψ. The other films length are modified by a quantity dr proportional to the applied strain.

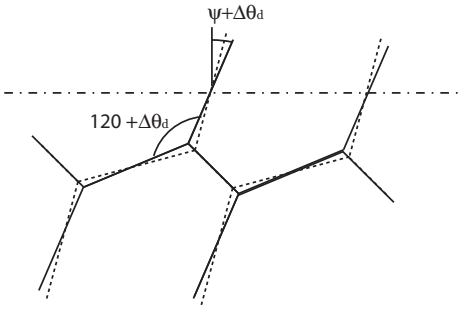

Figure 15. Effect of the dynamic contact angle correction on the deformation of a 2D hexagonal structure. Contrary to the classical quasistatic deformation (dashed line), the angle of the central Plateau border is no longer 120°. This deviation induces an additional rotation of the vertical line of an angle equal to the dynamic correction $\Delta\theta_d$.

[27]. Several models have been proposed to couple surface rheology to bulk foam mechanical response [4,30,31]. Here, our approach will be limited to a perturbative version of the Princen model.

This model pictures the foam as a 2D regular hexagonal lattice (figure 14(a)). Taking into account Plateau rule and the surface conservation of each cell, Princen derives the modification of lengths and orientations of the different films associated with an imposed quasistatic shear strain ϵ (figure 14(b)), from which he derives various mechanical quantities.

The angle Ψ of the initially vertical films as well as the film length variation dr can be expressed as a function of ϵ (see figure 14(b)):

$$\Psi = \frac{1}{2}\epsilon \tag{28}$$

$$\frac{dr}{r} = \frac{\sqrt{3}}{2}\epsilon \tag{29}$$

The shear stress on a horizontal line (indicated in figure 14(b)) can be evaluated by considering that each film crossing this line carries a contribution $F = 2\gamma\sin(\Psi)$. Since the width of a unit cell is $r\sqrt{3}$, the stress σ is written:

$$\sigma = F = \frac{2\gamma}{r\sqrt{3}}\sin(\Psi) \approx \frac{2\gamma}{r\sqrt{3}}\Psi \tag{30}$$

This allows one to write the shear modulus as:

$$G_0 = \frac{\sigma}{2\epsilon} = \frac{1}{\sqrt{3}}\frac{\gamma}{r} \tag{31}$$

The system is now submitted to an oscillating strain $\epsilon(t) = \epsilon_0\cos(\omega t)$. At finite oscillating frequency, one expects the Plateau rule to no longer be obeyed, and a correction $\Delta\theta_d(t)$ has to be added to the angle Ψ (see figure 15). By analogy with the double bubble measurements, we define A' and A'' such as:

$$\Delta\theta_d(t) = A'(\omega)\frac{dr}{r}\cos(\omega t) + A''(\omega)\frac{dr}{r}\sin(\omega t) \tag{32}$$

In the limit where the structure is weakly modified with regards to its equilibrium configuration (i.e. $\Delta\theta_d << \Psi$), the expression of dr/r provided by Princen (equation 29) remains valid to the first order. Substituting ψ by $\psi + \Delta\theta_d$ in equation 30 yields a corrected foam modulus which complex form now writes:

$$G^* = G_0[1 + \sqrt{3}(A' + iA")] \tag{33}$$

It should be noticed that this result is independent of the physical origin of the viscoelastic process which sets A' and A". With the solution used in the present study, it appears that the viscoelastic behavior of the films is responsible for the observed deviation to Plateau rule. But one might expect for other systems that the dominating effect is the viscous dissipation localized in the Plateau border. Regardless of this underlying mechanism, the frequency diagram obtained by the double bubble angular measurement directly provides the contribution of the film and Plateau border rheology to the foam modulus.

One limitation of this approach however needs to be underlined. The Princen model of foam elasticity is based on a perfectly regular network. In a real foam, r is largely distributed and one expects A' and A" to depend on the relative lengths of the films connecting the given vertex. One is actually confronted with the same averaging problem when trying to evaluate the macroscopic modulus μ of a disordered film network. This structure parameter should control the prefactor of $A' + iA$". But this limitation should still allow one to compare different systems (with different film rheological properties) provided that the foam structure is identical (same polydispersity).

Conclusion

A device has been developed to measure the contact angle between two soap bubbles in static and dynamic adhesion. This set-up allows us to confirm the existence of a negative line tension associated with the presence of a Plateau border at the intersection of three soap films: the static contact angle is systematically larger than 120° and the deviation amplitude can be quantitatively predicted given the central film radius and volume of the Plateau border. By varying the distance between bubbles, one can modulate the radius r_c of the central film. This induces a further deviation of the contact angle $\Delta\theta_d$ which

maximum value scales linearly with the amplitude of $\Delta r_c/r_c$. The amplitude and phase shift of $\Delta\theta_d$ with regards to $\Delta r_c/r_c$ has been systematically studied as a function of the modulation frequency.

The resulting phase diagram exhibits a transition from a viscous to an elastic regime with a crossover at a frequency of order 1rad.s^{-1}. This behavior of the double bubble cannot be deduced in a straightforward way from measurements of the film rheology obtained by single oscillating bubble measurements since exchanges can occur between adjacent surfaces. We constructed a model taking into account flows af surfactants from both the bulk phase and the adjacent surfaces for each monolayer. This leads to an expression of the angular module as a function of the dilational module and a characteristic time τ. Two limiting models correspond to extreme values of $\omega\tau$: the first one considers the three films in the double bubble experiment as being independently stretched and overestimate the stored and dissipated energy in the oscillating experiment. The second one corresponds to the situation in which surfactant layers are free to slide over one another and underestimates the experimental measurements.

In order to test this hypothesis, we intend to modulate the rheological properties of the surfactant monolayer and the bulk solution. Surface shear viscosity can be increased by adding dodecanol in the solution. In contrast, the interstitial film can be rendered more viscous by increasing glycerol concentration or by adding soluble polymers such as PEO (Polyethylene Oxide).

We have illustrated the possibility to use these angular measurements as a way to predict the contribution of the films and vertices to macroscopic foam rheology. The proposed approach is based on a perturbative version of the Princen 2D regular foam model. It is therefore extremely naive and will need further work in order to be adapted to 3D foams and to take into account structural disorder. However, it suggests that this type of geometrical measurements might provide most of the relevant information. In particular, it integrates the different modes of energy dissipation, including the viscous drag associated with the Plateau borders motion. In order to test these ideas, such dynamical adhesion data need to be confronted to standard rheological measurements on 3D foams for various chemical solutions.

We woud like to thank K.Brakke for his help with Surface Evolver simulations as well as J.-F. Géminard, I. Cantat, S. Cohen-Addad and R.Höhler for fruitful discussions.

References

1. S.A. Khan, C.A. Schnepper, R.C. Armstrong, J. Rheol. **32**(1), 69 (1988)
2. D. Weaire, S. Hutzler, *The Physics of Foams* (Oxford University Press, New York, 1999)
3. R. Höhler, S. Cohen-Addad, Journal of Physics: Condensed Matter **17**, R1041 (2005)
4. D. Buzza, C.Y. Lu, M. Cates, Journal de Physique II **5**(1), 37 (1995)
5. L. Schwartz, H. Princen, Journal of Colloid and Interface Science **118**(1), 201 (1987)
6. J. Lucassen, M. Van den Tempel, Journal of Colloid and Interface Science **41**(3), 491 (1972)
7. J. Lucassen, M. Van den Tempel, Chemical Engineering Science **27**(3), 1283 (1972)
8. V. Bergeron, Journal of Physics: Condensed Matter **11**, R215 (1999)
9. H. Fruhner, K.D. Wantke, Colloids and Surfaces, A: Physicochemical and Engineering Aspects **114**, 53 (1996)
10. H. Fruhner, K.D. Wantke, K. Lunkenheimer, Colloids and Surfaces, A: Physicochemical and Engineering Aspects **162**, 193 (1999)
11. K.D. Wantke, H. Fruhner, Journal of Colloid and Interface Science **237**(2), 185 (2001)
12. P. Aussillous, D. Quéré, Europhysics Letters **59**(3), 370 (2002)
13. I. Cantat, R. Delannay, Physical Review E **67**(3), 031501 (2003)
14. N. Denkov, V. Subramanian, D. Gurovich, A. Lips, Colloids and Surfaces, A: Physicochemical and Engineering Aspects **263**, 129 (2005)
15. E. Terriac, J. Etrillard, I. Cantat, Europhysics Letters **74**(5), 909 (2006)
16. M. Durand, H.A. Stone, Physical Review Letters **97**(22), 226101 (4) (2006)
17. H.M. Princen, Journal of Colloid and Interface Science **91**(1), 160 (1983)
18. J. Plateau, *Statique Expérimentale et Théorique des Liquides Soumis aux Seules Forces Moléculaires* (Clemm, Paris, 1873)
19. M. Fortes, M. Rosa, Journal of Colloid and Interface Science **241**(1), 205 (2001)
20. J. Rodriguez, B. Saramago, M. Fortes, Journal of Colloid and Interface Science **239**, 577 (2001)
21. J.C. Géminard, A. Zywocinski, F. Caillier, P. Oswald, Philosophical Magazine Letters **84**(3), 199 (2004)
22. M. Fortes, P. Teixeira, Philosophical Magazine Letters **85**(1), 21 (2005)
23. M. Fortes, P. Teixeira, Physical Review E **71**, 051404 (2005)
24. A. Neimark, M. Vignes-Adler, Physical Review E **51**(1), 788 (1995)
25. G. Han, A. Dussaud, B. Prunet-Foch, A. Neimark, M. Vignes-Adler, Journal of Non-Equilibrium Thermodynamics **25**, 325 (2000)
26. K. Brakke, Experimental Mathematics **1**, 141 (1992)
27. S. Cohen-Addad, R. Höhler, Y. Khidas, Physical Review Letters **93**(2), 028302 (2004)
28. D. Langevin, Advances in Colloid and Interface Science **88**, 209 (2000)
29. J. Lucassen, Faraday Discussions of the Chemical Society **59**, 76 (1975)
30. D. Edwards, H. Brenner, D. Wasan, *Interfacial Transport Processes and Rheology* (Butterworth-Heinemann, 1991)
31. D. Stamenovic, Journal of Colloid and Interface Science **145**(1), 255 (1991)